Arabian Journal of Chemistry (2015) xxx, xxx–xxx

King Saud University

Arabian Journal of Chemistry

www.ksu.edu.sa
www.sciencedirect.com

ORIGINAL ARTICLE

Effects of aluminum on amyloid-beta aggregation in the context of Alzheimer's disease

Qiulan Zhang [a], Fangyuan Zhang [a], Yongnian Ni [a,b,*], Serge Kokot [c]

[a] College of Chemistry, Nanchang University, Nanchang 330031, China
[b] State Key Laboratory of Food Science and Technology, Nanchang University, Nanchang 330047, China
[c] School of Chemistry, Physics and Mechanical Engineering, Science and Engineering Faculty, Queensland University of Technology, Brisbane 4001, Australia

Received 12 March 2015; accepted 13 June 2015

KEYWORDS

Alzheimer's disease;
β-Amyloid peptides;
Spectroscopy;
Chemometrics

Abstract Alzheimer's disease (AD) is one of the most common age-associated pathologies, which inevitably leads to dementia and death. The aggregation of β-amyloid (Aβ) peptides on plaques in brain tissue is strongly associated with AD. The possible link between aluminum and AD still remains controversial. In this work, the aggregation of Aβ40 induced by Al(III) was investigated with the use of the fluorescence quenching method, UV–visible and circular dichroism spectroscopies as well as the atomic force microscopy technique. The results demonstrated that Al(III) induced the transformation of the initial random coil structure to the β-sheet configuration in the Aβ40 peptides. These structural changes facilitated the aggregation of Aβ40. Also, the binding constant was calculated with the use of the multivariate curve resolution-alternating least squares (MCR-ALS) chemometrics method.

1. Introduction

Alzheimer's disease (AD) is the most common neurodegenerative disease, marked by clinical symptoms such as a decline in cognitive skills, behavioral changes, irreversible memory loss, and language impairment (Mattson, 2004). This illness is estimated to affect approximately 2% of the population in industrialized countries (Rauk, 2009). The pathological markers of AD are the presence of extracellular amyloid plaques and intracellular neurofibrils because they can form tangles (NFTs) (Chiti and Dobson, 2006). The major risk factor known for AD is age; about 95% of the AD cases have no clear pattern of inheriting the disease, and it appears that interactions of both the genetic and environmental factors contribute to the etiology of AD (Migliore and Coppede, 2009). The exact mechanism leading to AD is still not established, and there is no preventative protocol and no effective therapies for AD. Thus, research in all aspects of AD is important because, in general, the aims are to obtain a more complete

* Corresponding author at: College of Chemistry, Nanchang University, Nanchang 330031, China. Tel./fax: +86 791 83969500.
E-mail addresses: ynni@ncu.edu.cn (Y. Ni), s.kokot@qut.edu.au (S. Kokot).
Peer review under responsibility of King Saud University.

Production and hosting by Elsevier

http://dx.doi.org/10.1016/j.arabjc.2015.06.019
1878-5352

understanding of the AD, which eventually would lead to its cure or at least a rational treatment.

Extracellular amyloid plaques are commonly referred to as the senile plaques (SP); they are mainly made up of β-amyloid (Aβ) peptides, which exist in fibrilar form (Lovell et al., 1998). Such peptides are made from the amyloid precursor protein (APP) by β- and γ-secretase enzymes; also, these peptides usually contain either 40 or 42 amino acids (Aβ40 and Aβ42), respectively. Aβ40 is the major product of the APP processing, while Aβ42 is the predominant component of the senile plaques (Chiti and Dobson, 2006). Thus, Aβ neurotoxicity could result from an amyloid fibrilar aggregatie, and it has been suggested that the Aβ-soluble (Aβs) oligomers are the principal neurotoxic agents, which, even at very low concentrations, are capable of inducing marked changes in neuronal long-term potentiation (LTP) as well as in cognitive impairment (Lesne et al., 2005). Aβ peptides undergo spontaneous self-aggregation. However, the origin of this phenomenon is still unclear. Thus, aggregation and the formation of oligomers of the Aβ molecules are ongoing topics of interest contributing to the etiology and pathogenesis of AD.

Postmortem brain biopsies of AD patients have shown that the aggregated Aβs contain high concentrations of the metals, Fe, Cu and Zn (Miller et al., 2006), and in general, the accumulating evidence strongly indicates that metal ions are physiological and pathological hallmarks of AD (Duce and Bush, 2010; Drew and Barnham, 2010; Molina et al., 2007). Research has suggested that some metal ions play a distinct role in the aggregation of Aβ (Bush, 2003; Ricchelli et al., 2006). These metal ions behave differently from those that form the slowly self-assembled aggregates; rather, they accelerate the dynamic aggregation of Aβ. Consequently, the acceleration of the dynamic aggregation process is likely to increase the neurotoxic effects on the neuron cells. Aluminum (Al) is the most widely distributed metal in the environment and is extensively used in daily life (Kumar and Gill, 2009). It is one of the metals that has a demonstrated human toxicity, and is highly neurotoxic. In this context, Al was suspected to be implicated in the progression of AD, when it was found to induce the formation of neuro-fibrilar tangles in the cerebrum of rabbits (Klatzo et al., 1965; Terry and Pena, 1965). However, over the years the role of Al in the etiology and pathogenesis of AD has been controversial. While Al(III) is known to aggregate in high concentrations in the AD amyloid deposits, studies concerned with the linkage between Al and AD have not reached consensus (Munoz, 1998; Zatta, 1993; Zatta et al., 2003). Consequently, the question of the link between Al (III) and AD remains of considerable interest (Walton, 2006).

The aims of this work were:

1. to investigate the effect of Al(III) in aqueous solution on the conformation and aggregation of Aβ, and to relate the findings to any effects on the AD;
2. to apply a chemometrics method of data analysis, namely multivariate curve resolution-alternating least squares (MCR-ALS) (Tauler, 1995), so as to explore whether this approach can extract qualitative and/or quantitative information, which otherwise is inaccessible to conventional methods.

2. Experimental section

2.1. Materials

Aβ40 peptides (>95% pure) were purchased from GL Biochem Ltd. (Shanghai). The lyophilized peptides (2.2 mg) were dissolved in dimethylsulfoxide (DMSO, 5.0 mL) and sonicated in a water bath for 5 min to solubilize any existing aggregates. This solution was diluted with water (5.0 mL) and filtered through a 0.45 μm filter. The concentration of Aβ40 was immediately determined by absorption spectroscopy ($\varepsilon = 1410\ cm^{-1}\ M^{-1}$) (Edelhoch, 1967). It was labeled a stock solution, which was kept in a refrigerator for further use. Thioflavin T (ThT) was purchased from Sigma (USA) and its stock solution was prepared by dissolving 63.8 mg of its crystals in 10 mL 0.01 mol L^{-1} Tris–HCl buffer (pH 7.4). The aluminum solution (6.0×10^{-1} mol L^{-1}) was prepared directly from aluminum chloride (Shanghai Reagent Factory, Shanghai). Tris–HCl buffer (pH 7.4) was prepared by mixing 50 mL 0.1 M 2-Amino-2-hydroxymethyl-propane-1,3-diol with 42 mL 0.1 M HCl, and diluted to 100 mL with water. All other reagents were of analytical grade and used without further purification. All solutions used in the experiments were adjusted with the Tris–HCl buffer (0.05 mol L^{-1}, pH 7.4) to 0.01 mol L^{-1}. Doubly distilled water was used throughout.

Four sample solutions, each diluted to 250 μL for experiments (Section 2.3.3 and 2.3.4), were prepared: (1) fresh Aβ40 solution (prepared by 120 μL 50 μM Aβ40 solution), (2) Aβ40 aggregates (prepared by 120 μL 50 μM Aβ40 solution), and (3) and (4) Aβ40 solution (prepared by 120 μL 50 μM Aβ40 solution) + Al(III) solution (0.56 mM and 1.12 mM, respectively). Here the Al(III) was added to facilitate the formation of Aβ aggregates. A suitable amount of Tris–HCl buffer was added to adjust the concentration of Tris–HCl to 0.01 mol L^{-1}. Samples 2, 3 and 4 were immersed in a water bath at 37 °C for 3 days before analysis. These samples were submitted to the following analyses: thioflavin T fluorescence, turbidity, circular dichroism and atomic force microscopy.

2.2. Apparatus

UV–vis absorption spectra were recorded with an Agilent 8453 spectrophotometer (Agilent Technologies, Santa Clara, CA, USA) using a 1.0 cm quartz cuvette. The fluorescence spectra were collected with an LS-55 luminescence spectrometer (Perkin–Elmer Instruments, Waltham, MA, USA) equipped with a thermostatic bath (Model ZC-10, Tianheng Instruments Factory, Ningbo, China) and a 1.0 cm quartz cuvette. Circular dichroism (CD) spectra were measured on a MOS-450/AF-CD spectrometer (Bio-Logic Co., Marseille, France) under constant nitrogen flush with the use of a 1.0 cm quartz cuvette. The spectra were collected from samples at pH 7.4 Tris–HCl buffer at room temperature (25 °C); all spectra were adjusted for any spectral contributions from the buffer. The atomic force microscopy (AFM) images were obtained with the use of an Agilent 5500 AFM (Agilent Technologies, Santa Clara, CA, USA) in the tapping mode. All the measurements were carried out at 25.0 ± 0.5 °C unless otherwise stated.

Please cite this article in press as: Zhang, Q. et al., Effects of aluminum on amyloid-beta aggregation in the context of Alzheimer's disease. Arabian Journal of Chemistry (2015), http://dx.doi.org/10.1016/j.arabjc.2015.06.019

2.3. Experimental procedure

2.3.1. Fluorescence quenching experiment

For this experiment, the fluorescence associated with Aβ40 was quenched by Al(III), and this effect was measured on the addition of Al(III) to the Aβ solution (3.56×1.0^{-6} mol L^{-1}). The Al(III) solution associated with this step were 0.0–7.5×10^{-6} mol L^{-1} added at intervals of 5.0×10^{-7} mol L^{-1}. The reaction conditions for each sample were as follows: the reaction medium was 0.01 mol L^{-1} Tris–HCl buffer and each solution was allowed to stand for 5 min prior to scanning. The spectroscopic scanning range was 260–500 nm (step of 2 nm, total 121 points) with an excitation wavelength of 260 nm. Thus total 16 spectra with 121 wavelengths were obtained.

2.3.2. Thioflavin T fluorescence measurements

An aliquot of a sample (100 μL) was added to a cuvette (1 cm), which contained ThT (1900 μL, 20 μM). This solution was allowed to stand for 5 min, and then a fluorescence spectrum was recorded at an excitation wavelength of 440 nm in the range of 420–620 nm.

2.3.3. UV–vis absorption experiments

A fresh 4.98×10^{-5} mol L^{-1} Aβ40 solution was prepared, and a 1.88×10^{-5} mol L^{-1} Al(III) solution was added to it sequentially from 0.0 at intervals of 3.13×10^{-6} mol L^{-1}. After each addition and thorough mixing, an absorption spectrum was recorded in the range of 200–900 nm.

The absorption spectra of the freshly prepared Aβ40, Aβ40 aggregates, and Al(III) induced Aβ40 aggregate solutions (see Section 2.1), were collected immediately; the absorbance at 405 nm was recorded and considered to represent the turbidity of the samples (Storr et al., 2007).

2.3.4. Circular dichroism spectra measurements

Sample solutions containing fresh Aβ40, Aβ40 oligomer, and Al(III) induced Aβ40 oligomer were scanned separately by the use of a MOS-450/AF-CD spectrometer in a 1.0 cm quartz cuvette over a wavelength range of 190–280 nm with a scanning speed of 1 nm s^{-1}.

2.3.5. Atomic force microscope study

Samples for the AFM images were prepared by depositing 10 μL of a sample solution of fresh Aβ40, Aβ40 oligomer, or Al(III) induced Aβ40 oligomer, on freshly cleaved mica plates (1.2 cm × 1.2 cm), which were dried overnight.

2.4. Chemometrics methods

Multivariate curve resolution–alternating least squares (MCR-ALS) is a well-known multivariate self-modeling curve resolution method of data analysis, (Tauler, 1995). It facilitates a bilinear decomposition of the experimental data matrix according to the following algebraic model:

$$\boldsymbol{D} = \boldsymbol{C}\,\boldsymbol{S}^{\mathrm{T}} + \boldsymbol{E} \quad (1)$$

where $\boldsymbol{D}$ is the experimental data matrix with dimensions, M (spectral objects)×N (wavelengths); $\boldsymbol{C}$ ($M \times F$) is the concentration profile matrix of F analytes in the samples; $\boldsymbol{S}^{\mathrm{T}}$ ($F \times N$) is the transposed matrix consisting of, for example, the emission spectra. The F rows of this matrix contain the pure spectra associated with the F species in the samples; $\boldsymbol{E}$ ($M \times N$) is the residuals matrix. The number of F values is estimated by rank analysis, with the use of singular value decomposition (SVD), principal component analysis (PCA), or other related techniques based on factor analysis, such as the evolving factor analysis (EFA) method (Gampp et al., 1986). The MCR-ALS procedure calculates the $\boldsymbol{C}$ and $\boldsymbol{S}$ matrices in turn by the least squares method, and the iterative process is repeated until convergence. When the number of species, F, and the initial estimates, which are required to initiate the iterative ALS procedure (Vives et al., 2000), have been extracted, the concentration profiles and the pure spectra of all the contributing species can be established by the MCR-ALS method.

3. Results and discussion

3.1. Investigation of the fluorescence quenching

When excited by 260 nm radiation, the Aβ40 peptides naturally fluoresce at 336 nm; this has been attributed to the absorption of the impinging radiation by the tyrosine residues (Rozga et al., 2010). The interaction between Al(III) and Aβ40 was investigated by monitoring the quenching of the tyrosine fluorescence (Fig. 1A, Section 2.3.1). As expected, the addition of Al(III) resulted in a decrease of this fluorescence, and an isoactinic point formed at 400 nm; this indicated that a chemical equilibrium existed in the system. Also, with the addition of Al(III), the fluorescence peak broadened with a slight blue shift; this suggested that on interacting with Al(III), the microenvironment around the tyrosine residues of Aβ40 was affected. To investigate the spectra further, they were converted to first derivatives; often this type of data transformation facilitates the separation of any overlapping peaks.

The first derivative profiles of the fluorescence spectra changed significantly on addition of the Al(III) (Fig. 1B). The positive profiles of the spectra indicated that initially there appeared to be only one band present (spectrum 1); this, however, began to split into two major bands, which decreased progressively in intensity. However, the intensity of this peak at the lower wavelength (288 nm) stabilized after about the tenth addition of Al(III), while the peak at about 315 nm became apparent after about the fourth addition of the Al(III). On further additions, this peak collapsed rapidly but it still could be discerned in the last few spectral profiles. Interestingly, from the 14 to 16th additions of Al(III), the intensity of this peak, although low, stabilized. In addition, when the first-derivative of each of peak was overlaid then the values of the spectral profiles were close to zero in the narrow wavelength range of 336–325 nm (see arrow, Fig. 1B). In the negative parts of the spectral profiles, there were no easily discernible profile changes but a non-zero crossing point was observed at about 338 nm, this means that the fluorescence spectral peaks were blue shifted, and the values of the tangent slope of each spectrum were almost equal at this wavelength. Overall, these observations indicated that the fluorescence emission spectra contained detailed information about the interaction of Al(III) and Aβ40, but in order to extract it, the spectral profiles had to be processed by a method such as MCR-ALS. This method is designed to extract quantitative and qualitative information from spectral data.

Please cite this article in press as: Zhang, Q. et al., Effects of aluminum on amyloid-beta aggregation in the context of Alzheimer's disease. Arabian Journal of Chemistry (2015), http://dx.doi.org/10.1016/j.arabjc.2015.06.019

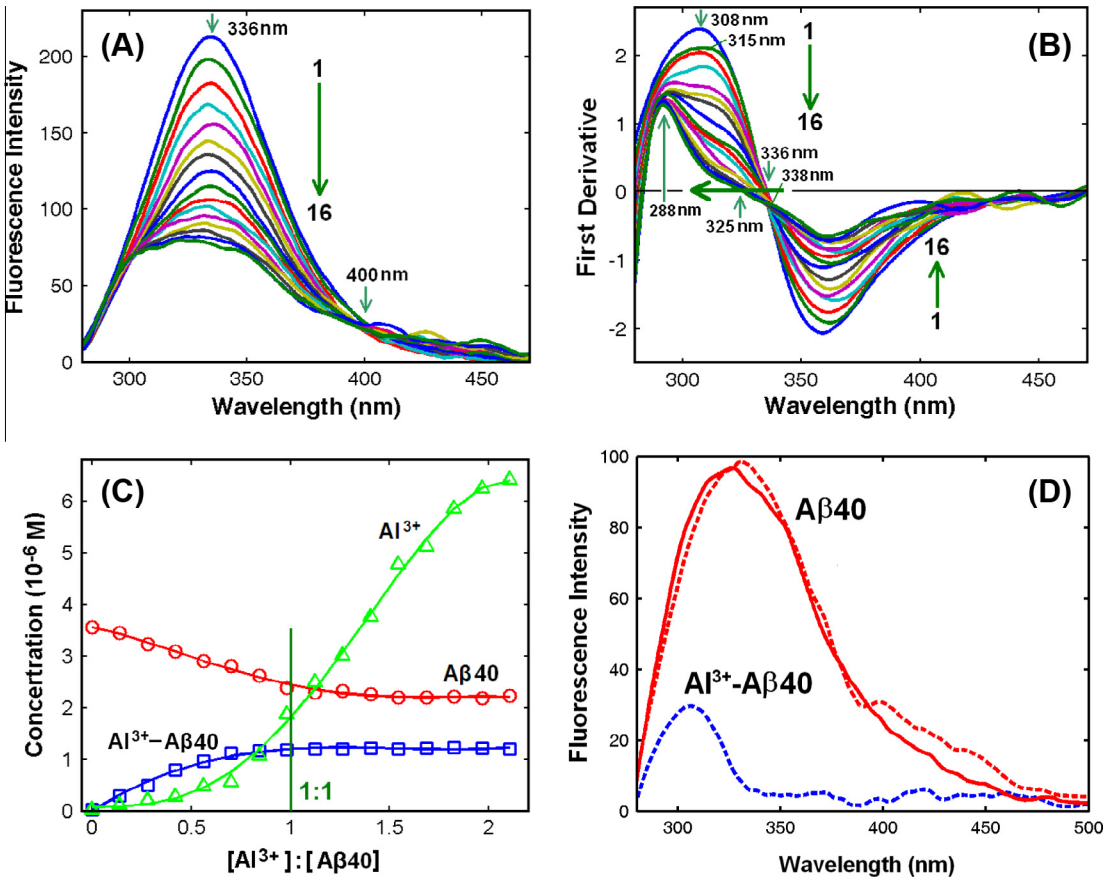

Figure 1 (A) Fluorescence emission spectra of Aβ40 (3.56×10^{-6} mol L^{-1}) after the addition of Al(III) (0–7.5×10^{-6} mol L^{-1} at intervals of 5.0×10^{-7} mol L^{-1}). (B) Derivative fluorescence emission spectra. (C) Concentration profiles of the Aβ40, Al(III) and Al(III)–Aβ40 analytes extracted from the fluorescence data matrix by MCR-ALS. (D) Spectral profiles of the Aβ40 and Al(III)–Aβ40 analytes extracted from the fluorescence data matrix (dashed line: extracted).

The spectral data matrix, ***D*** with dimension of 16 (spectral objects) × 121 (wavelengths), was first submitted to EFA so as to extract the significant factors and three were obtained in this case. This is consistent with the presence of Al(III), Aβ40 and the Al(III)–Aβ40 complex; relative concentration profiles of each chemical component involved in the interaction were then obtained by the MCR-ALS method. Such information together with the known initial concentration and the application of the mass balance principal, produced the real quantitative concentration profile of each reaction component, by using constraints, such as non-negativity and unimodality (Fig. 1C). The initial drop in concentrations of the Al(III) and Aβ40 qualitatively supported the formation of an Al(III)–Aβ40 complex, and its change in concentration, quantitatively supported the buildup of this complex until it reached a kinetic equilibrium position when [Al(III)]: [Aβ40] ≈ 1; the binding constant, K_a, was estimated as follows:

$$K_a = [\text{Al(III)–A}\beta40]/[\text{Al(III)}][\text{A}\beta40] \quad (2)$$

where [Al(III)–Aβ40], [Al(III)] and [Aβ40] are the estimated concentrations for the complex, free Al(III) and free Aβ40, respectively at each point of the concentration profiles. The [Al(III)]: [Aβ40] for the complex was about 1 (Fig. 1C), and the value of K_a was calculated to be 2.63×10^5 mol L^{-1} according to Eq. (2). This indicated that there was a strong interaction force between the Al(III) and Aβ40. These observations suggested that Al(III) could accelerate the kinetic aggregation of Aβ40. The value of K_a is qualitatively similar to values reported in the literature, in which other techniques were applied (Asandei et al., 2014). It should be kept in mind that although previously reported metal affinities of the various Aβ peptides seemed to vary appreciably, this can be accounted for by taking into considerations the different experimental conditions used in different studies, e.g., different models reported the use of different buffers to influence the binding of metals, and the initial aggregation states of the peptide (Warmlander et al., 2013).

From the finally resolved pure spectra (Fig. 1D), qualitative information about the nature of the complex was extracted. The obtained fluorescence spectra (dashed line) were compared well with the measured spectra (solid line). It should be emphasized that the fluorescence spectra for the Al(III)–Aβ40 complex (dashed line of Al(III)–Aβ40, Fig. 1D) and the concentration profiles of the Al(III)–Aβ40 complex in the kinetic binding procedure, were obtained with the use of MCR-ALS method. Such spectra are quite difficult to obtain

without chemometrics modeling, i.e. by conventional methods. These spectra indicated that Aβ40 is able to form binary complexes with Al(III).

3.2. Effect of Al(III) on Aβ40 aggregation

The effect of Al(III) on Aβ40 aggregation was first assessed with the use of UV–vis absorption (see Section 2.3.3); this method is for exploring structural changes in biopolymers and for confirming any formation of ligand–protein complexes (Bi et al., 2005; Kandagal et al., 2006). The Aβ40 peptides show a characteristic absorption peak at 285 nm, and consequently when an Al(III) containing solution was added to the sample, the peak intensity decreased at 285 nm (Fig. 2A). This result indicated that in this context, Al(III) may cause some changes to the peptide's structure and content in Aβ40. In relation to these changes, an important issue to investigate is whether or not the addition of Al(III) is associated with the formation of Aβ40 aggregates such as β- or amorphous types (Ha et al., 2007). In this context, any turbidity of the sample indicates a change in optical density of the analyte solution. Consequently, turbidity measurements can be used to indicate the different types of Aβ40 aggregates, including β- and amorphous ones (Ha et al., 2007). In this work, turbidity was estimated indirectly with the use of UV–vis absorption spectroscopy at 405 nm (Fig. 2B). For a fresh Aβ40 solution, the turbidity was quite low (0.004). However, when the Aβ40 solution was allowed to stand for three days at 37 °C in the presence of Al(III), turbidity increased substantially (0.031). This indicated that Al(III) can facilitate the aggregation of Aβ40 amyloids.

To assess the degree of aggregation, a well-known aggregation marker, thiazine dye (ThT), was utilized (see Section 2.3.2) (Khurana et al., 2005). This dye specifically binds to the aggregated β-sheet fibrils common to amyloid structures, and this binding should lead to a significant enhancement in fluorescence of ThT according to the amount of the amyloid peptides present (Khurana et al., 2005). Thus, a fresh Aβ40 solution showed only a weak response to ThT, (Fig. 3; curve 1), which indicated that Aβ40 exists almost unchanged, and when the Aβ40 solution was allowed to stand at 37 °C, it behaved similarly, (Fig. 3; curve 2), which indicated that only a small number of β-aggregates formed by the self-assembly process of the peptides. In contrast, when the Al(III) solution was added to either of the two above cases, the fluorescence at 480 nm increased substantially, which indicated that Aβ40 in the presence of Al(III), was transformed from its initial state to the β-structure (Fig. 3; curve 3). Furthermore, when Al(III) at a higher concentration was added to the above two solutions, fluorescence intensity increased even more (Fig. 3; curve 4). Thus, combining the above observations from the two experiments, it is clear that Al(III) facilitates the aggregation of the Aβ40 peptides.

Circular dichroism (CD) spectroscopy provides general indication for the increase in the β-structure content that accompanies the aggregation of the Aβ peptide. To investigate the structural changes of the peptide, CD spectroscopy in the far UV region (190–240 nm) was applied to detect any changes in the secondary structure of Aβ40 alone or in the presence of 0.56 mM and 1.12 mM of Al(III) solutions, respectively. To provide further information on the aggregation of Aβ40 induced by Al(III), the changes to the secondary structure of Aβ40 were investigated with the use of CD spectroscopy (see Section 2.3.4 and Fig. 4). It is well known that the

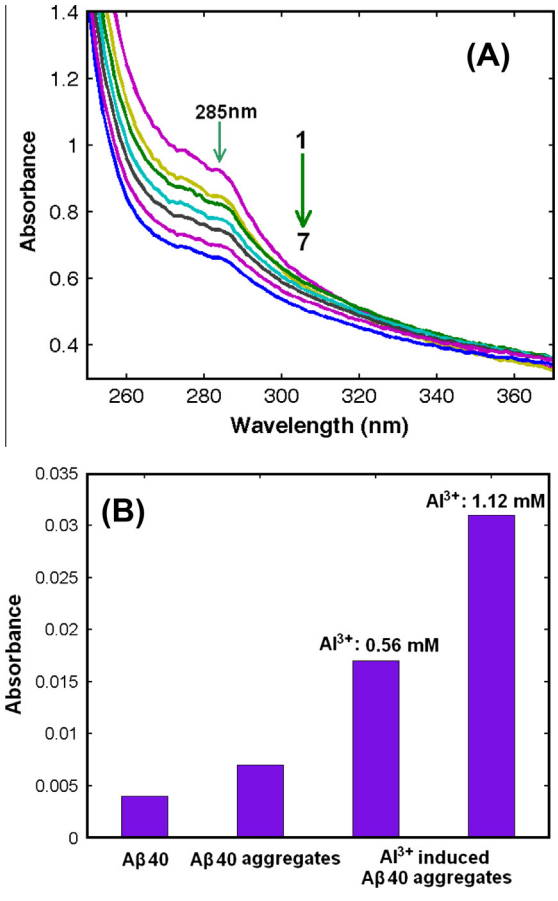

Figure 2 (A) UV–vis absorbance spectra of Aβ40 (4.98×10^{-5} mol L^{-1}) in the presence of various concentrations of Al(III) (0–1.88×10^{-5} mol L^{-1} at intervals of 3.13×10^{-6} mol L^{-1}). (B) Turbidity (A_{405}) of fresh Aβ40, Aβ aggregates, and Al(III) induced Aβ aggregates (sample preparation see Section 2.1).

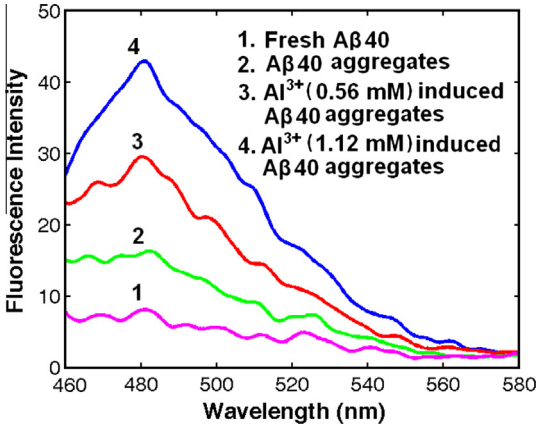

Figure 3 ThT fluorescence spectra of fresh Aβ40 and the Aβ40 solution in the absence and presence of Al(III) after the reaction period (samples prepared as in Section 2.1).

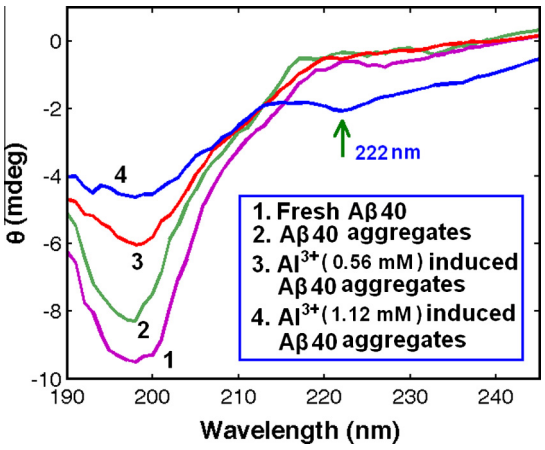

Figure 4 CD spectra of Aβ40 and the Aβ40 solution in the absence and presence of Al(III) after incubation (samples prepared as in Section 2.1).

characteristic spectral peak for the β-sheet structure appears at about 222 nm at which point, it has minimum ellipticity (Dai et al., 2015; Petrlova et al., 2012). The untreated Aβ40 amyloid sample produced a typical CD spectrum of the random coil conformation (curves 1 and 2) (Tickler et al., 2005), while, in the case of the Aβ40 sample solution, which was treated with Al(III), the ellipticity of the random coil conformation was found to be less negative (curves 3 and 4), and a characteristic spectrum of the β-sheet structure appeared in the last spectrum (see arrow).

These observations suggest that the presence of Al(III) facilitates the transformation of the Aβ40 peptides from the initial random coil structure to the β-sheet protein. The conclusion obtained here is consistent with the above observations based on monitoring the ThT fluorescence.

In addition, the size variations associated with the above molecular interactions, and the surface morphology of the untreated Aβ40, Aβ40 aggregates, and the Al(III) induced Aβ40 aggregate samples were analyzed with the use of a tapping mode atomic force microscopy (AFM) (see Section 2.3.5). The topography image for the Aβ40 molecules adsorbed on mica showed that this substance formed many tiny particles on the surface (Fig. 5A). After treatment at 37 °C for 3 days, much larger particles, which are much fewer in number than in the first case, were observed; on close examination, they appeared to have rough edges, which is a feature that perhaps is indicative of such particles being formed by the self-assembly process (Fig. 5B). When the Aβ40 sample was treated with Al(III) many, non-uniform, tightly packed fibrils were distributed on the mica surface in a disorderly manner (Fig. 5C). These observations are consistent with those reported for Zn and Cu in similar circumstances (Chen

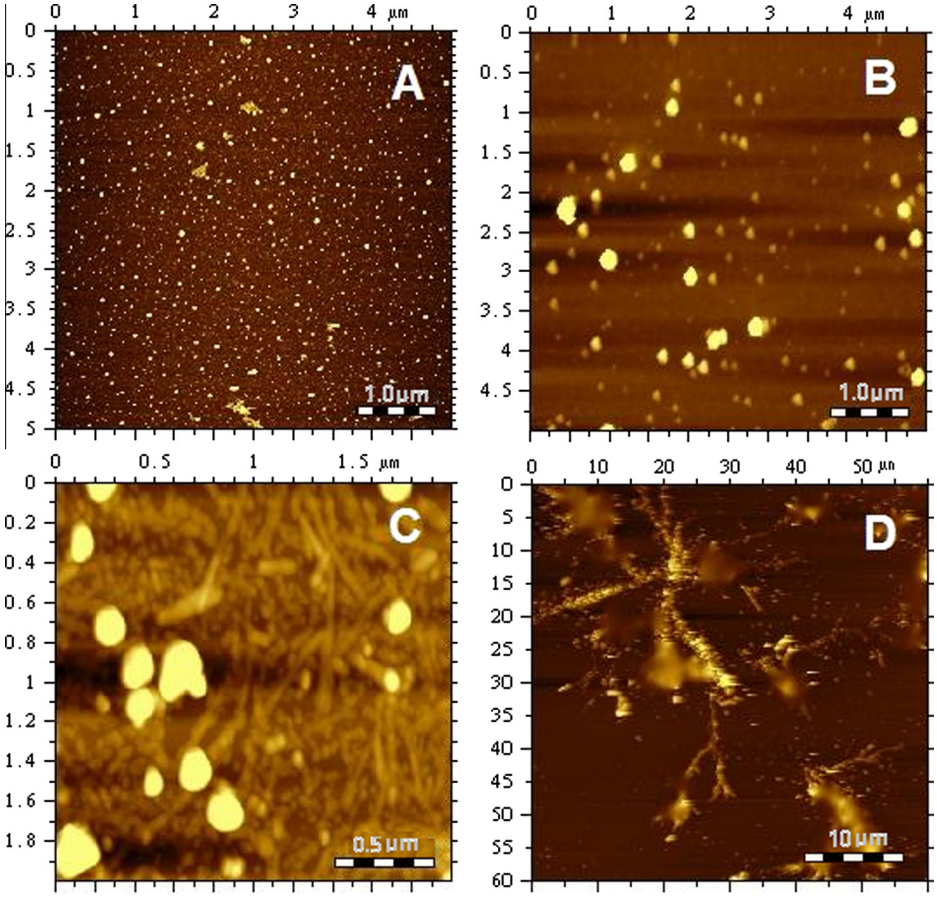

Figure 5 AFM images of fresh Aβ40: (A) Aβ aggregates, (B) and Al(III) induced Aβ aggregates (C and D). Concentration of Al(III) in sample D is higher than in C (prepared as in Section 2.1), and scan area is 2.0 μm × 2.0 μm.

et al., 2009). Interestingly, when Al(III) at a higher concentration, was used to treat an Aβ40 sample, the morphology was quite different – the Aβ40 aggregate, was quite similar to that observed in Fig. 5B, and appeared to pack into relatively long, rigid rods (Fig. 5D); although these rods are larger, they are otherwise quite similar to the fibrils referred to in Fig. 5C. These observations suggest that Al(III) can induce the formation of Aβ40 aggregates, and may act as a mediator in the formation of fibrillar amyloid plaques in AD; clearly, the concentration of the Al(III) solution is an important aspect to consider when assessing the effect of Al(III) on the Aβ40 aggregation. This work suggests that amyloid aggregates will form in the presence of a wide range of concentrations. However, it would appear that the morphology of these aggregates will differ widely as a function of Al(III) concentration. These aggregates appear to range from tiny particles to relatively large ones, and they self-assemble into shapes ranging from short strings to relatively long and apparently rigid rods.

4. Conclusion

It has been demonstrated with the use of fluorescence, UV–vis, CD, and AFM techniques that Al(III) can play an important role as a mediator in the formation of fibrillar amyloid plaques in Alzheimer's disease. The above analytical methods provided collectively the information, which enabled the establishment of reactants and products as well as the physical parameters; these characterized the reaction mechanisms and kinetic rates as well as the associated equilibrium constants. Furthermore, some quantitative and qualitative information, such as the binding constant of the interaction between Al(III) and Aβ40, and the spectrum of the binding complex of Al(III)-Aβ40 can be obtained with the use of the MCR-ALS chemometrics method. An important aspect of this work was the concentration of Al(III) because it was an important variable which affected the Aβ40 aggregation process.

Acknowledgment

The authors gratefully acknowledge the financial support of this study by the National Natural Science Foundation of China (NSFC-21065007), and the State Key Laboratory of Food Science and Technology of Nanchang University (SKLF-ZZA-201302 and SKLF-ZZB-201303).

References

Asandei, A., Iftemi, S., Mereuta, L., Schiopu, I., Luchian, T., 2014. Probing of various physiologically relevant metals: amyloid-β peptide interactions with a lipid membrane-immobilized protein nanopore. J. Membr. Biol. 247, 523–530.

Bi, S.Y., Song, D.Q., Tian, Y., Zhou, X., Liu, Z.Y., Zhang, H.Q., 2005. Molecular spectroscopic study on the interaction of tetracyclines with serum albumins. Spectrochim. Acta A 61, 629–636.

Bush, A.I., 2003. The metallobiology of Alzheimer's disease. Trends Neurosci. 26, 207–214.

Chen, T.T., Wang, X.Y., He, Y.F., Zhang, C.L., Wu, Z.Y., Liao, K., Wang, J.J., Guo, Z.J., 2009. Effects of cyclen and cyclam on zinc (II)- and copper (II)-induced amyloid β-peptide aggregation and neurotoxicity. Inorg. Chem. 48, 5801–5809.

Chiti, F., Dobson, C.M., 2006. Protein misfolding, functional amyloid, and human disease. Annu. Rev. Biochem. 75, 333–366.

Dai, X.L., Hou, W.Q., Sun, Y.X., Gao, Z.L., Zhu, S.G., Jiang, Z.F., 2015. Chitosan oligosaccharides inhibit/disaggregate fibrils and attenuate amyloid β-mediated neurotoxicity. Int. J. Mol. Sci. 16, 10526–10536.

Drew, S.C., Barnham, K.J., 2010. The heterogeneous nature of Cu^{2+} interactions with Alzheimer's amyloid-beta peptide. Acc. Chem. Res. 44, 1146–1155.

Duce, J.A., Bush, A.L., 2010. Biological metals and Alzheimer's disease: implications for therapeutics and diagnostics. Prog. Neurobiol. 92, 1–18.

Edelhoch, H., 1967. Spectroscopic determination of tryptophan and tyrosine in proteins. Biochemistry 6, 1948–1954.

Gampp, H., Maeder, M., Meyer, C.J., Zuberbuhler, A.D., 1986. Calculation of equilibrium constants from multiwavelength spectroscopic data-IV: model-free leaser-squares refinement by use of evolving factor analysis. Talanta 33, 943–951.

Ha, C., Ryu, J., Park, C.B., 2007. Metal ions differentially influence the aggregation and deposition of Alzheimer's β-amyloid on a solid template. Biochemistry 46, 6118–6125.

Kandagal, P.B., Ashoka, S., Seetharamappa, J., Vani, V., Shaikh, S.M.T., 2006. Study of the interaction between doxepin and human serum albumin by spectroscopic methods. J. Photochem. Photobiol. A 179, 161–166.

Khurana, R., Coleman, C., Ionescu-Zanetti, C., Carter, S.A., Krishna, V., Grover, R.K., Roy, R., Singh, S., 2005. Mechanism of thioflavin T binding to amyloid fibrils. J. Struct. Biol. 151, 229–238.

Klatzo, I., Wisniewski, H., Streicher, E., 1965. Experimental production of neurofibrillary degeneration: 1. Light microscopic observations. J. Neuropathol. Exp. Neurol. 24, 187–199.

Kumar, V., Gill, K.D., 2009. Aluminum neurotoxicity: neurobehavioural and oxidative aspects. Arch. Toxicol. 83, 965–978.

Lesne, S., Koh, M.T., Kotilinek, L., Kayed, R., Glabe, C.G., Yang, A., Gallagher, M., Ashe, K.H., 2005. A specific amyloid-β protein assembly in the brain impairs memory. Nature 440, 352–357.

Lovell, M.A., Robertson, J.D., Teesdale, W.J., Campbell, J.L., Markesbery, W.R., 1998. Copper, iron and zinc in Alzheimer's disease senile plaques. J. Neurol. Sci. 158, 47–52.

Mattson, M.P., 2004. Pathways towards and away from Alzheimer's disease. Nature 430, 631–639.

Migliore, L., Coppede, F., 2009. Genetics, environmental factors and the emerging role of epigenetics in neurodegenerative diseases. Mutat. Res. 667, 82–97.

Miller, L.M., Wang, Q., Telivala, T.P., Smith, R.J., Lanzirotti, A., Miklossy, J., 2006. Synchrotron-based infrared and X-ray imaging shows focalized accumulation of Cu and Zn co-localized with β-amyloid deposits in Alzheimer's disease. J. Struct. Biol. 155, 30–37.

Molina, H.F., Hider, R.C., Gaeta, A., Williams, R., Francis, P., 2007. Metals ions and neurodegeneration. Biometals 20, 639–654.

Munoz, D.G., 1998. Is exposure of aluminum a risk factor for the development of Alzheimer's disease? Arch. Neurol. 55, 737–739.

Petrlova, J., Kalai, T., Maezawa, I., Altman, R., Harishchandra, G., Hong, H.S., Bricarello, D.A., Parikh, A.N., Lorigan, G.A., Jin, L.W., 2012. The influence of spin-labeled fluorene compounds on the assembly and toxicity of the A beta peptide. PLoS One 7, e35443.

Rauk, A., 2009. The chemistry of Alzheimer's disease. Chem. Soc. Rev. 38, 2698–2715.

Ricchelli, F., Buggio, R., Drago, D., Salmona, M., Forloni, G., Negro, A., Tognon, G., Zatta, P., 2006. Aggregation/fibrillogenesis of recombinant human prion protein and Gerstmann–Sträussler–Scheinker disease peptides in the presence of metal ions. Biochemistry 45, 6724–6732.

Rozga, M., Kloniecki, M., Dadle, M., Bal, W., 2010. A direct determination of the dissociation constant for the Cu(II) complex of amyloid β 1–40 peptide. Chem. Res. Toxicol. 23, 336–340.

Please cite this article in press as: Zhang, Q. et al., Effects of aluminum on amyloid-beta aggregation in the context of Alzheimer's disease. Arabian Journal of Chemistry (2015), http://dx.doi.org/10.1016/j.arabjc.2015.06.019

Storr, T., Merkel, M., Song-Zhao, G.X., Scott, L.E., Green, D.E., Bowen, M.L., Thompson, K.H., Patrick, B.O., Schugar, H.J., Orvig, C., 2007. Synthesis, characterization, and metal coordinating ability of multifunctional carbohydrate-containing compounds for Alzheimer's therapy. J. Am. Chem. Soc. 129, 7453–7463.

Tauler, R., 1995. Multivariate curve resolution applied to second order data. Chemom. Intell. Lab. Syst. 30, 133–146.

Terry, R.D., Pena, C., 1965. Experimental production of neurofibrillary degeneration: 2. Electron microscopy, phosphatase histochemistry and electron prose analysis. J. Neuropathol. Exp. Neurol. 24, 200–210.

Tickler, A.K., Smith, D.G., Ciccotosto, G.D., Tew, D.J., Curtain, C.C., Carrington, D., Masters, C.L., Bush, A.I., Cherny, R.A., Cappai, R., Wade, J.D., Barnham, K.J., 2005. Methylation of the imidazole side chains of the Alzheimer disease amyloid-beta peptide results in abolition of superoxide dismutase-like structures and inhibition of neurotoxicity. J. Biol. Chem. 280, 13355–13363.

Walton, J.R., 2006. Aluminum in hippocampal neurons from humans with Alzheimer's disease. Neurotoxicology 27, 385–394.

Warmlander, S., Tiiman, A., Abelein, A., Luo, J., Jarvet, J., Soderberg, K.L., Danielsson, J., Garslund, A., 2013. Biophysical studies of the amyloid β-peptide: interactions with metal ions and small molecules. ChemBioChem 14, 1692–1704.

Vives, M., Gragallo, R., Tauler, R., 2000. Multivariate extension of the continuous variation and mole-ratio methods for the study of the interaction of intercalators with polynucleotides. Anal. Chim. Acta 424, 105–114.

Zatta, P., 1993. Controversial aspects of aluminium(III) accumulation and subcompartmentation in Alzheimer's disease. Trace. Elem. Med. 10, 120–128.

Zatta, P., Lucchini, R., Van Rensburg, S.J., Taylor, A., 2003. The role of metals in neurodegenerative processes: aluminum, manganese and zinc. Brain Res. Bull. 62, 15–28.

Please cite this article in press as: Zhang, Q. et al., Effects of aluminum on amyloid-beta aggregation in the context of Alzheimer's disease. Arabian Journal of Chemistry (2015), http://dx.doi.org/10.1016/j.arabjc.2015.06.019